PAPER

Check for updates

Tuning flexibility in metal–organic frameworks *via* linker per-fluorination: revisiting the adsorption-induced breathing of MIL-53(Al)

Virginia Guiotto,[a] Maria Sole Notari,[b] Jacopo Perego,[c] Diletta Morelli Venturi, [de]
Francesca Nardelli, [fg] Alberto Ricchebuono, [ah] Silvia Bordiga, [a] Susana Garcia,[i]
Marco Taddei, [gj] Matteo Signorile, [a] Angiolina Comotti,[c] Lucia Calucci, *[fj]
Ferdinando Costantino *[b] and Valentina Crocellà *[a]

We present the first comprehensive investigation of the complex, multi-step adsorption-induced breathing behaviour of F_4-MIL-53(Al), the recently discovered analogue of MIL-53(Al) with a per-fluorinated linker. Through a systematic characterisation approach performed by combining *in situ* Powder X-ray Diffraction (PXRD), *in situ* Fourier Transform Infrared (FTIR) and Solid State Nuclear Magnetic Resonance (SS-NMR) spectroscopies with sorption analyses, we unveil the impact of fluorination on framework flexibility, adsorption properties, and phase transitions, offering fresh perspectives into the structure–property relationships governing Metal–Organic Framework (MOF) dynamic porosity. Compared to the non-fluorinated MIL-53(Al), F_4-MIL-53(Al) exhibits a different water affinity, with uptake remaining below 1 mmol g^{-1} up to 60% relative humidity. Above this threshold, PXRD reveals a two-step expansion of the F_4-MIL-53(Al) unit cell, contrasting the typical contraction observed in MIL-53(Al). Volumetric CO_2 adsorption at different temperatures displays non-hysteretic step-shaped isotherms for F_4-MIL-53(Al), generated by a CO_2-induced structural expansion also confirmed by *in situ* PXRD analysis. These findings highlight the crucial role of fluorination in tuning host–guest interactions, modifying water affinity while preserving and revisiting dynamic porosity and, more broadly, provide new insights into the molecular-level design of responsive fluorinated MOFs for gas separation and storage.

[a]Dipartimento di Chimica, Centro di Riferimento NIS, Unità di Ricerca INSTM, Università di Torino, Via G. Quarello 15/A and Via P. Giuria 7, 10125 Torino, Italy. E-mail: valentina.crocella@unito.it

[b]Dipartimento di Chimica, Biologia e Biotecnologie, Unità di Ricerca INSTM, Università degli Studi di Perugia, Via Elce di Sotto 8, 06123 Perugia, Italy. E-mail: ferdinando.costantino@unipg.it

[c]Dipartimento di Scienza dei Materiali, Unità di Ricerca INSTM, Università degli Studi di Milano-Bicocca, Via R. Cozzi 55, 20125 Milano, Italy

[d]Institute of Inorganic Chemistry Christian-Albrecht Universität zu Kiel, Max-Eyth-Straße 2, 24118 Kiel, Germany

[e]Kiel Nano, Surface and Interface Science KiNSIS, Christian-Albrecht Universität zu Kiel, Christian-Albrecht-Platz 4, 24118 Kiel, Germany

[f]Istituto di Chimica dei Composti OrganoMetallici, Consiglio Nazionale delle Ricerche, Via Giuseppe Moruzzi 1, 56124 Pisa, Italy. E-mail: lucia.calucci@pi.iccom.cnr.it

[g]Dipartimento di Chimica e Chimica Industriale, Unità di Ricerca INSTM, Università di Pisa, Via Giuseppe Moruzzi 13, 56124 Pisa, Italy

[h]IFP Energies Nouvelles, Rond-Point de l'Echangeur de Solaize, BP 3, 69360 Solaize, France

[i]Research Centre for Carbon Solutions, Heriot-Watt University, EH14 4AS, Edinburgh, UK

[j]Centro per l'Integrazione della Strumentazione Scientifica dell'Università di Pisa (CISUP), Lungarno Pacinotti 43/44, 56126 Pisa, Italy

Introduction

The ability of a solid to reversibly switch between contracted and expanded phases, commonly referred to as 'breathing' or 'sponge-like' behaviour, is a remarkable feature of Soft Porous Crystals (SPCs),[1] a class of flexible crystalline porous materials that undergo phase changes in response to external stimuli such as gas adsorption, temperature and pressure.[2,3] Among SPCs, Metal–Organic Frameworks (MOFs) have emerged as a class of materials capable of exhibiting significant structural transformations. Among these materials, MIL-53 has been established as the prototype of the breathing MOF family, laying the foundation for decades of research into dynamic porosity.[1,4–10]

The relevance of flexible materials extends far beyond fundamental structural chemistry. For example, adsorption-induced flexibility of MOFs has major implications for gas separation applications and energy-efficient adsorption processes. Indeed, breathing is often reflected in peculiar S-shaped isotherms, which possibly enhance working capacity and reduce energy consumption in pressure- and temperature-swing adsorption processes.[1,11] Therefore, controlling and

predicting such transformations remains an extraordinary challenge.[12]

First reported by Serre et al. in 2002,[13] the MIL-53 framework consists of 1,4-benzenedicarboxylate (bdc) linkers bridging trivalent metal cations (M^{III}). Among its many variants, MIL-53(Al) is the most extensively studied,[14] due to Al abundance (8.2 wt% of the Earth's crust) and low cost (1.8 € per kg).[15] Moreover, Al^{III} forms strong bonds with carboxylic linkers, allowing the design of MOFs with exceptional thermal and hydrolytic stability. This makes MIL-53(Al) a rare example of MOF produced on a large scale and commercialised by BASF under the trade name of Basolite A100.[16]

The flexibility of MIL-53(Al) has been extensively studied, revealing its ability to undergo phase transitions in response to external stimuli.[8,17–20] For instance, exposure to atmospheric moisture triggers a contraction from a large-pore (lp) to a narrow-pore (np) phase due to the formation of hydrogen bonds between H_2O molecules and the MOF framework (the structural model of the np phase is reported in Fig. S1A).[14] This transition results in a unit cell volume contraction up to 40%. Beyond water, other guest molecules, including SO_2,[17] Xe,[18] CH_4[19] and CO_2,[19,21] have been shown to induce a similar flexible behaviour.

Despite its well-documented flexibility, precise control over the breathing behaviour of MIL-53(Al) remains elusive. A powerful strategy to tune flexibility in MOFs is chemical functionalisation of the linker. In 2015, Munn et al. demonstrated how incorporating various substituents on the bdc linker (–CH_3, –Cl, –Br, –NH_2, –NO_2, –$(OH)_2$, –CO_2H) profoundly alters the structural response of MIL-53(Al),[22] revealing a direct correlation between electronic effects and steric constraints of the substituents and host–guest interactions.[22]

Among the countless possible linker modifications, fluorination emerges as a particularly intriguing route for tuning the flexibility of MOFs. The high electronegativity and the strong electron-withdrawing character of fluorine atoms significantly modify the textural properties, the framework rigidity and the adsorption properties of fluorinated MOFs. Indeed, it has been proved how fluorination of bdc enhances torsional flexibility of the ligand by altering the twist angle between the benzene ring and the carboxylate groups of many MOFs.[23] Furthermore, Nagaoka et al. demonstrated with DFT methods that the planarity of the bdc system mainly depends on electrostatic interactions (e.g. H-bonding). In bdc, the strong intramolecular electrostatic interaction between the oxygen of the carboxylate groups and the hydrogen atoms on the phenyl ring stabilises the planarity of the moiety, while the repulsive interaction between oxygen and fluorine atoms causes the rotation of the phenyl ring out of the carboxylate plane.[24]

Van der Voort and co-workers synthesised and investigated mono- and para-difluorinated MIL-53(Al), proving that even a single fluorine substitution substantially modifies the mechanism of breathing. Unlike pristine MIL-53(Al), which contracts upon water adsorption, monofluorinated and difluorinated MIL-53(Al) do not show water-induced phase transitions.[25,26]

Recently, we synthesised a fully fluorinated MIL-53(Al) variant [F_4-MIL-53(Al)] using a solvent-free approach.[27] Our preliminary studies disclosed a reversible temperature-induced transition ($np_{F_4} \rightarrow lp_{F_4}$) of F_4-MIL-53(Al), occurring at 513 K with minimal hysteresis ($\Delta T \sim 5$ K). This is in contrast with the behaviour of MIL-53(Al), which exhibits a slow and broadly hysteretic ($\Delta T \sim 200$ K) breathing transition, as reported by Liu and co-authors.[8] In general, the true impact of fluorination on adsorption-induced flexibility remains largely unexplored. Traditional ex situ techniques often fail to capture transient intermediate states and dynamic structural transformations, leading to an incomplete understanding of host–guest interactions. For this reason, we present here an advanced, multi-technique in situ investigation of the response of F_4-MIL-53(Al) to the adsorption of different probes, i.e., H_2O, CO_2, Ar, N_2 and CO, in comparison with that of MIL-53(Al). Our approach exploits in situ and ex situ Powder X-ray Diffraction (PXRD) to track real-time structural evolution, in situ Infrared (IR) and Solid State Nuclear Magnetic Resonance (SS-NMR) spectroscopies to acquire molecular-scale insights into framework-adsorbate interactions, and volumetric adsorption analysis to identify and quantify adsorption-driven transitions. By integrating these complementary techniques, we disclosed the complex multi-step flexible response of F_4-MIL-53(Al) to adsorption.

Results and discussion

H_2O-induced flexibility

Water affinity is a key point in MOFs characterisation. Indeed, water can destabilise many MOFs or compete with other gases, lowering the adsorption performances.[28] In flexible frameworks, water adsorption/desorption can induce phase transitions.[5,14,29] Therefore, understanding MOFs structural response to relative humidity and identifying the material phase before sorption measurements that require a pre-activation step (i.e. involving water removal) is essential.

The crystallinity of MIL-53(Al) [labelled hereafter as H_4-MIL-53(Al)] and F_4-MIL-53(Al) after the synthesis was checked by PXRD (Fig. S2). Both frameworks are stable in their respective np phases prior to any activation treatment.[14,27] The unit cell volume of the np_{F_4} phase is 1292.1 Å^3, about 30% more expanded than the np_{H_4} phase of H_4-MIL-53(Al) (863.9 Å^3).[14,27] The structural models of both MOFs are reported in Fig. S1A and B.

The morphology of the two MOFs was evaluated by Field Emission Scanning Electron Microscopy (FE-SEM). At the micrometre scale, H_4-MIL-53(Al) exhibits well-defined prismatic crystals with regular and smooth surfaces and big particle size, indicating a high crystallinity. In contrast, F_4-MIL-53(Al) displays a more disordered morphology, characterized by the agglomeration of thicker, plate-like crystallites. This difference is further highlighted at higher magnifications, where the roughness of the F_4-MIL-53(Al) surface becomes clearly visible (Fig. S3).

The H_2O-induced flexibility of H_4-MIL-53(Al) is well-known. SS-NMR and PXRD studies discovered that water physisorbed from the atmosphere interacts with different sites from both the organic linker and the bridging Al–OH–Al groups in the

inorganic units.[14,30,31] However, the SS-NMR study concluded that the hydrogen atoms of H_2O interact with the carboxylate groups of the framework through H-bonds, triggering the contraction of the rhombic channels of H_4-MIL-53(Al), affording the narrow pore np_{H_4} phase. Upon water removal, an expansion of the pores is observed, leading to the large pore lp_{H_4} phase.[14]

In contrast, PXRD patterns of as synthesised and evacuated F_4-MIL-53(Al) (Fig. S4) indicate that no transition occurs upon removal of water adsorbed from the atmosphere (Relative Humidity – RH < 70%). The refinement of the stable phases before and after activation was studied in a previous work, revealing the same orthorhombic np_{F_4} phase in both cases.[27]

In situ IR spectra of H_4-MIL-53(Al) and F_4-MIL-53(Al) were recorded during evacuation at room temperature (RT) (Fig. S5). The analyses reveal two different responses upon desorption of atmospheric water. The IR profile of F_4-MIL-53(Al) remains unaltered upon evacuation, except for the disappearance of the band at 1145 cm^{-1}, associated to the $\delta(\mu\text{-OH})$ bending mode of the inorganic unit in interaction with physisorbed water.[32] The low intensity of this band and of the broad signal in the OH stretching region (inset of Fig. S5A) indicates that F_4-MIL-53(Al) adsorbs a low quantity of water when exposed to atmospheric moisture. In contrast, the IR spectrum of H_4-MIL-53(Al) undergoes significant changes upon activation (Fig. S5B). In particular, the strong decrease of the intensity of the band between 1200 cm^{-1} and 1050 cm^{-1}, associated with the same $\delta(\mu\text{-OH})$ mode,[33] can be attributed to the presence of a larger amount of H_2O inside the channels of H_4-MIL-53(Al) before activation. Again, the larger quantity of physisorbed water can be detected by observing the –OH stretching region (inset of Fig. S5B).

The behaviour upon evacuation significantly differs between H_4-MIL-53(Al) and F_4-MIL-53(Al). When channels are empty, H_4-MIL-53(Al) exhibits the lp_{H_4} phase while fluorine atoms decorating the rhombic channels of F_4-MIL-53(Al) stabilise the evacuated structure in the closed np_{F_4} phase.

Van der Voort *et al.* previously demonstrated that mono- or di-fluorination of the bdc linker strongly affects the H_2O induced breathing behaviour of MIL-53(Al).[25,26] Specifically, their studies reported that mono-fluorinated MIL-53(Al) stabilises the lp phase in both hydrated (from moisture) and dehydrated phases, while pF_2-MIL-53(Al) favours the np phase regardless of hydration state.[25,26] The behaviour of F_4-MIL-53(Al) resembles that of pF_2-MIL-53(Al), suggesting that the presence of more than two fluorine atoms further stabilises the contracted np phase and prevents the expansion of the cell upon removal of hydrogen-bonded water molecules. However, it is worth noticing that fluorinated MIL-53(Al) MOFs reported by Van der Voort *et al.* were synthesised using dimethylformamide (DMF) rather than water and this may significantly alter the flexible behaviour of the resulting materials.[34]

The water affinity of F_4-MIL-53(Al) was assessed by gravimetric adsorption/desorption isotherms collected at 303 K (Fig. 1A). The presence of four fluorine atoms significantly enhances the material hydrophobic character within the 0–70% RH range, as evidenced by a low H_2O uptake of less than 2 mmol g^{-1}. This interesting property was recently noticed by Zhang
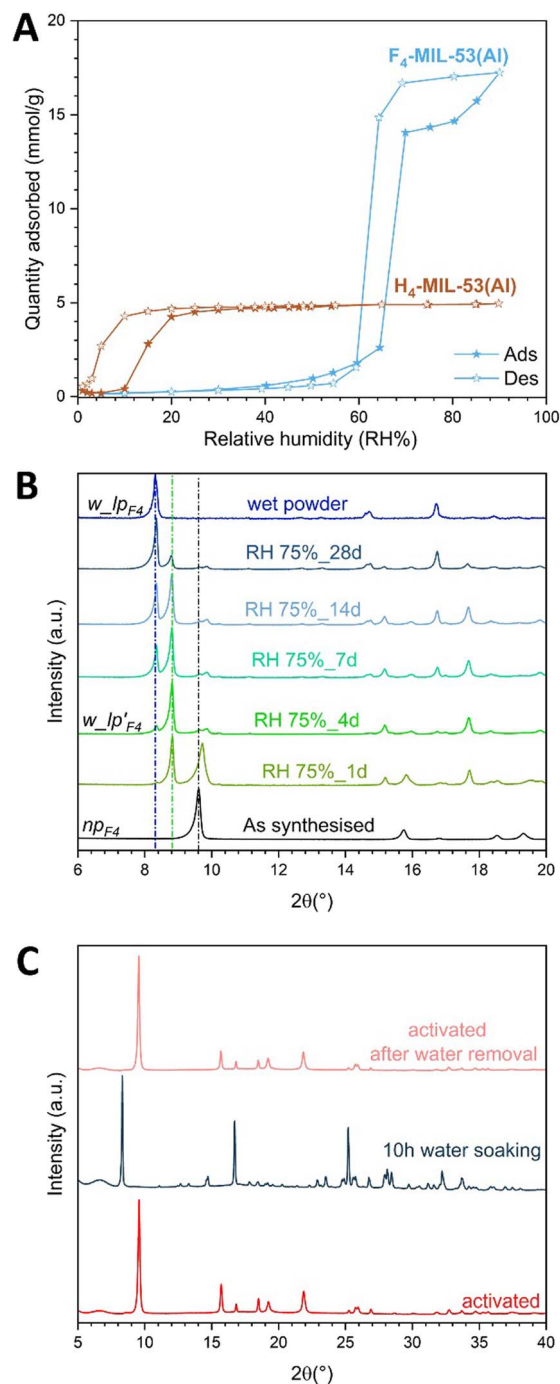

Fig. 1 (A) Gravimetric H_2O adsorption (full symbols) and desorption (empty symbols) isotherms collected at 303 K on H_4-MIL-53(Al) (brown) and F_4-MIL-53(Al) (blue). (B) Comparison of PXRD patterns of F_4-MIL-53(Al) at different RH: powder exposed to ambient atmosphere (black, as-synthesized. RH < 75%), powder exposed for several days at 75% of RH (green and light blue), powder wetted with water (blue RH ≈ 100%). The dashed lines refer to the 110 reflection which is diagnostic of the shrinkage and breathing behaviour of F_4-MIL-53(Al). (C) Comparison between the PXRD patterns of F_4-MIL-53(Al) after activation (red), soaked in water for 10 h (dark blue) and after water removal with vacuum at 298 K (pale red).

32448 | *J. Mater. Chem. A*, 2025, **13**, 32446–32459

This journal is © The Royal Society of Chemistry 2025

et al., who exploited it to facilitate the selective permeation of *n*-butanol from water using a mixed matrix membrane containing F_4-MIL-53(Al) as a filler.[35]

Interestingly, although water uptake remains minimal at RH levels below 70%, the isotherm reveals a flexible response of F_4-MIL-53(Al) when the material is exposed to RH values above 70%.[35]

In particular, as synthesised F_4-MIL-53(Al) is in the closed phase (np_{F_4}). Upon hydration at 75% RH for 1 day (RH 75%_1d), a new, more expanded phase is formed and coexists with the np_{F_4} one, as testified by the appearance of the main reflection at lower 2θ values (8.81° 2θ). After 4 days at 75% RH (RH 75%_4d), the pattern only shows the reflections of the new expanded phase ($w\_lp'_{F_4}$, where "w" stands for "water"), which is now the prevailing phase. After 7 days (RH 75%_7d), a second, even larger pore phase is detected, indicated by the appearance of a new peak at $2\theta = 8.32°$. This larger phase ($w\_lp_{F_4}$) coexists with the $w\_lp'_{F_4}$ one for an extended period. Indeed, even after 28 days at 75% RH (RH 75%_28d), a mixture of $w\_lp'_{F_4}$ and $w\_lp_{F_4}$ phases is observed. The single final $w\_lp_{F_4}$ phase is only detected when the MOF powder is wetted with liquid water. The whole PXRD sequence shows that the $np_{F_4} \rightarrow w\_lp'_{F_4}$ transition occurs with a relatively fast kinetics (just one day). The subsequent $w\_lp'_{F_4} \rightarrow w\_lp_{F_4}$ conversion progresses much more slowly, probably requiring a longer time under these RH conditions or higher RH values for completion, as testified by the pattern collected on the wet sample (blue pattern in Fig. 1B).

To identify the $w\_lp_{F_4}$ crystal structure, PXRD measurements were also performed on F_4-MIL-53(Al) after soaking in water for 10 h using a hermetic chamber to avoid evaporation. The PXRD pattern (Fig. 1C, dark blue) displays a dramatic shift of the first diffraction peak towards lower 2θ angles compared to the activated structure (from 9.62° to 8.32°), corresponding to a d_{110} spacing of 10.62 Å (see Fig. S1C), associated with the squaring of the rhombus of the wine-rack structure of F_4-MIL-53(Al). The unit cell can be refined using the Le Bail method in the monoclinic crystal system (space group $C2/c$, Fig. S6 and Table S1). The unit cell shows a doubling of the c axis with lattice parameters $a = 15.5820(8)$ Å, $b = 15.8985(9)$ Å and $c = 13.2991(7)$ Å, angle $\beta = 114.688(2)°$ and $V = 2993.5(3)$ Å. The PXRD pattern collected after evacuation of the water-soaked sample at RT proves the reversibility of the phase transition (Fig. 1C, pale red). It is important to note that, considering the cell volume, the final uptake of 18 mmol g^{-1} (see isotherm in Fig. 1A) cannot be completely attributed to water molecules inside the channels of the $w\_lp_{F_4}$ phase. Instead, the presence of water on the MOF external surface must be hypothesized.

Multinuclear (^{1}H, ^{19}F, ^{13}C, and ^{27}Al) SS-NMR spectroscopy was also employed to investigate the structure of F_4-MIL-53(Al) and its changes upon H_2O adsorption in comparison with H_4-MIL-53(Al). Activated F_4-MIL-53(Al) shows single ^{1}H and ^{19}F isotropic signals from μ_2-OH groups (2.97 ppm) and linker fluorine atoms (−145.1 ppm), respectively (Fig. 2A, B and Tables S2, S4). In the ^{19}F–^{13}C CP-MAS spectrum, three signals are observed at 117.2, 145.4, and 166.2 ppm ascribable, respectively, to quaternary, fluorinated, and carboxylic carbons of the linkers (Fig. 2C and Table S4). The ^{27}Al DE-MAS spectrum shows

a signal typical of the octahedral environment of Al in the $[AlO_4(OH)_2]$ centres, with isotropic chemical shift, $\delta = 3.37$ ppm, quadrupolar coupling constant, $C_Q = 9.24$ MHz, and asymmetry parameter, $\eta_Q = 0.07$ (Fig. 2D and Table S3).

^{1}H, ^{19}F, and ^{27}Al spectra were collected during the hydration of activated F_4-MIL-53(Al), first at 75% RH and then at 100% RH, to delve into the $np_{F_4} \rightarrow w\_lp'_{F_4}$ and $w\_lp'_{F_4} \rightarrow w\_lp_{F_4}$ transitions, respectively (Fig. 2, S7 and S8).

During the hydration at 75% RH, the ^{1}H signal first broadens and moves to higher chemical shift. After three days, two peaks are observed in the spectrum, at 3.75 and 5.70 ppm, the intensities of which progressively increase by prolonging the hydration time, reaching an 8 : 1 ratio at equilibrium after 11 days (Fig. S7A and Table S2). Since, according to the sample weight, 4 H_2O molecules per formula were adsorbed by F_4-MIL-53(Al) at this stage, in agreement with the H_2O adsorption isotherm (Fig. 1A), the signal at 5.70 ppm is ascribed to μ_2-OH and that at 3.75 ppm to H_2O protons.[36] The ^{19}F isotropic signal slightly shifts (from −145.1 to −144.7 ppm) at the beginning of the hydration. Then, a second broad signal appears at −139.2 ppm, which increases in intensity as the hydration progresses, while the first signal disappears (Fig. S7B and Table S4). The ^{27}Al signal shifts and broadens during the hydration at 75% RH, showing a superposition of two sub-spectra in the intermediate stages (Fig. S8) and a single signal with $\delta = 5.67$ ppm, $C_Q = 10.85$ MHz, and $\eta_Q = 0.07$ when the equilibrium is reached (Fig. 2D and Table S3). The evolution of the ^{1}H, ^{19}F and ^{27}Al spectra with the hydration time indicates that the $w\_lp'_{F_4}$ phase progressively forms at the expense of the np_{F_4} one. The ^{1}H and ^{27}Al NMR data suggest that, in the $w\_lp'_{F_4}$ phase, the μ_2-OH groups strongly interact with H_2O molecules. The δ and C_Q values of hydrated F_4-MIL-53(Al) are similar to those found for hydrated H_4-MIL-53, here (Fig. S9C and Table S3) and in the literature,[14,30,37–40] but η_Q is smaller (0.07 instead of 0.14). These findings indicate that, while the interaction of H_2O with μ_2-OH groups changes the charge distribution on Al along the Al–OH direction for both MOFs, thus increasing δ and C_Q, only for H_4-MIL-53(Al) a change of symmetry of the Al environment in the coordination plane of carboxylate groups occurs, resulting in an increase of η_Q.[37,38] These findings are further corroborated by the ^{13}C NMR spectra (Fig. 2C, S9B and Table S4). Indeed, only slight changes of carbon chemical shifts are observed upon hydration for F_4-MIL-53(Al), whereas for H_4-MIL-53(Al) a considerable shift of the carboxylate carbon signal is associated to interactions with H_2O and structural rearrangement at the $lp_{H_4} \rightarrow np_{H_4}$ transition.[14,39–41] Conversely, hydration of F_4-MIL-53(Al) results in a change of the ^{19}F isotropic chemical shift (Fig. 2B and Table S4), suggesting interactions between fluorine atoms and H_2O and/or a conformational change of the linker.

Slight changes are detected in the ^{19}F SS-NMR spectrum after further exposing the F_4-MIL-53(Al) sample to 100% RH for two days (Fig. S7B), indicating that no significant structural modifications occur at the $w\_lp'_{F_4} \rightarrow w\_lp_{F_4}$ transition. Indeed, this spectrum matches the one recorded on wet F_4-MIL-53(Al) (Fig. 2B, S7B and Table S4) exhibiting the $w\_lp_{F_4}$ phase according to PXRD data. On the other hand, the ^{1}H DE MAS spectrum presents some changes upon further hydration. After
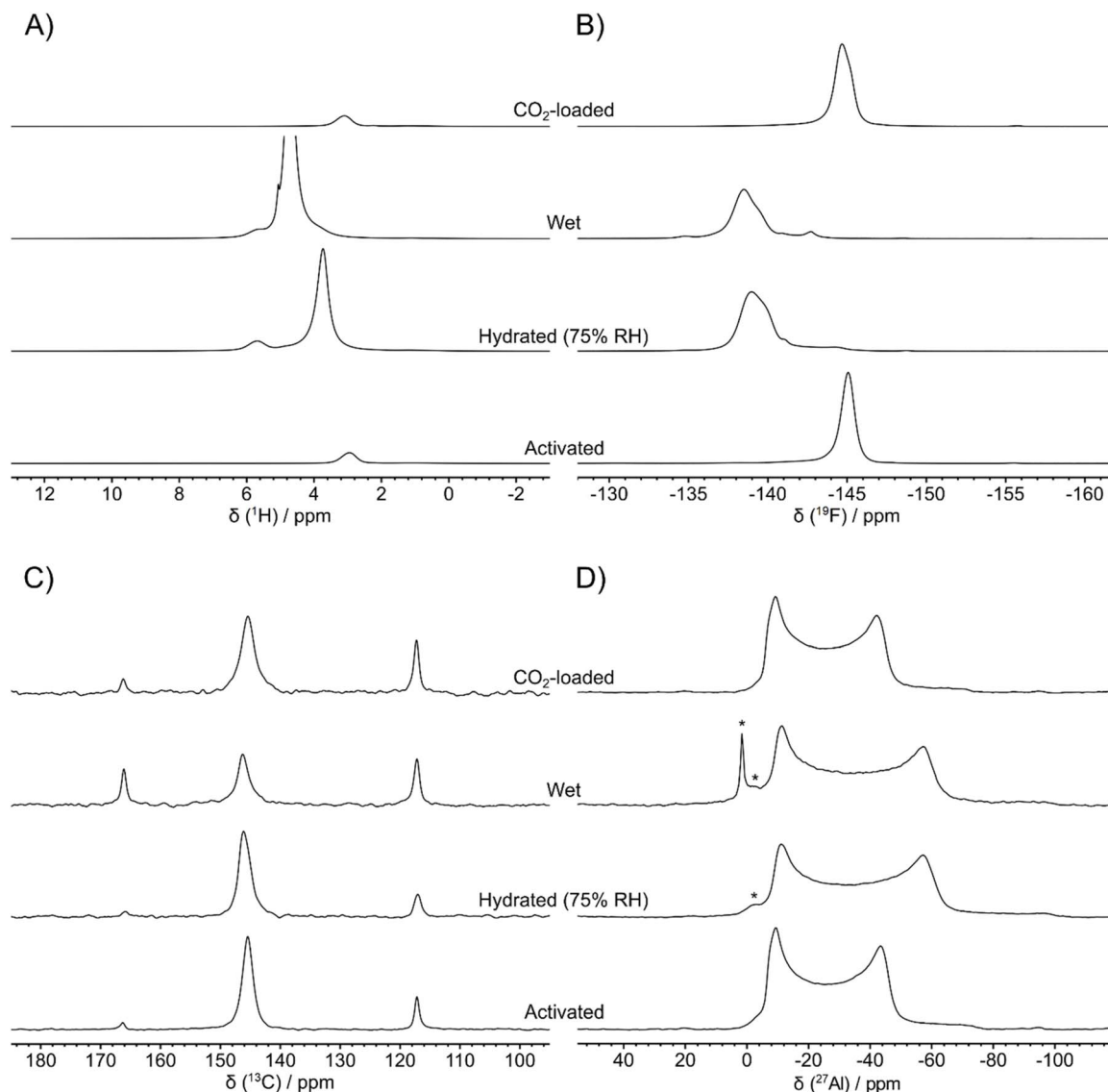
This journal is © The Royal Society of Chemistry 2025

J. Mater. Chem. A, 2025, **13**, 32446–32459 | **32449**

Fig. 2 (A) ^{1}H DE-MAS, (B) ^{19}F DE-MAS, (C) ^{19}F–^{13}C CP-MAS, and (D) ^{27}Al DE-MAS NMR spectra of activated, hydrated (75% RH for 11 days), wet, and CO_2-loaded F_4-MIL-53(Al). Asterisks in ^{27}Al DE-MAS NMR spectra indicate signals of impurities.

$5H_2O$ molecules per MOF formula are adsorbed by F_4-MIL-53(Al) based on the sample weight, three signals are observed with 1 : 8 : 2 relative intensities, ascribable to μ_2-OH (5.60 ppm) and to H_2O molecules inside (3.85 ppm) and outside (4.85 ppm) the MOF channels (Fig. S7A and Table S2). This indicates that only 4 H_2O molecules per formula can be accommodated within the F_4-MIL-53(Al) channels, the excess water residing on the MOF external surface.

Evaluation of textural properties

Volumetric adsorption isotherms were measured to assess the textural properties of F_4-MIL-53(Al) and H_4-MIL-53(Al). Initially, N_2 at 77 K was used. However, due to its quadrupolar moment and its ellipsoidal shape, N_2 is not an ideal probe for surfaces decorated with functional groups. Ar at 87 K, with its spherical shape, inert nature, and smaller kinetic diameter, offers a better

alternative.[42,43] Adsorption/desorption isotherms are shown in Fig. S10, with BET equation fittings in Fig. S11 and S12. Both samples exhibit Type I isotherms.[43] The specific surface area (SSA) of H_4-MIL-53(Al), determined with the two probes, is 1590 m^2 g^{-1} (N_2) and 1437 m^2 g^{-1} (Ar), respectively, consistent with literature values for this MOF.[14] For F_4-MIL-53(Al), SSA values are 1082 m^2 g^{-1} (N_2) and 1025 m^2 g^{-1} (Ar). Its lower SSA compared to the protonated analogue can be due to the presence of bulkier fluorine atoms oriented towards the pore centre. Indeed, when normalised by molecular mass per unit formula, the surface areas of the two MOFs in m^2 $mmol^{-1}$ become comparable (299 m^2 $mmol^{-1}$ for H_4-MIL-53 against 287 m^2 $mmol^{-1}$ for F_4-MIL-53). The difference in SSA values derived from N_2 and Ar isotherms in both samples is likely due to the quadrupolar nature of N_2, which leads to an overestimation of the surface area.[44]

32450 | *J. Mater. Chem. A*, 2025, **13**, 32446–32459

This journal is © The Royal Society of Chemistry 2025

Adsorption-induced flexibility at cryogenic temperatures

Surprisingly, the Ar and N_2 isotherms of F_4-MIL-53(Al) in a semi-logarithmic scale reveal a peculiar multi-step trend, whereas a single step due to micropore filling is observed for H_4-MIL-53(Al) (Fig. 3). Fluorinated micropores are filled in the 0–0.01 relative pressure (p/p_0) range *via* a multi-step mechanism, with pressure thresholds for each step varying slightly with the probe due to differences in gas-framework interactions. Considering water adsorption results, the existence of multiple intermediate phases linking the initial np_{F_4} phase [activated F_4-MIL-53(Al)] to the lp_{F_4} phase can be inferred. Recently, molecular simulations on H_4-MIL-53(Al) disclosed a $np_{H_4} \rightarrow lp_{H_4}$ transition induced by Ar adsorption at cryogenic temperatures, but the presence of multiple thermodynamically stable phases was excluded.[45]

A flexible response of F_4-MIL-53(Al) is also observed upon CO adsorption at 77 K. CO was selected as a more interacting probe, with a kinetic diameter similar to that of N_2 (3.8 Å and 3.6 Å, respectively). CO produces a multi-step isotherm (Fig. 3B) with fewer steps than the other probes. To test whether highly

interactive molecules trigger breathing in H_4-MIL-53(Al), an attempt to collect a CO isotherm was made. However, CO diffusion was too slow, and after *ca.* 100 h, only a few data points were collected. Notably, even the N_2 isotherm of H_4-MIL-53(Al) takes ~55 h, confirming slow kinetics for larger molecules at cryogenic temperatures. However, for CO, its stronger interaction with H_4-MIL-53(Al) could be responsible for excessively long equilibration times, making the measurement experimentally unfeasible.

CO_2 – induced flexibility

Boutin *et al.*[19] reported that H_4-MIL-53(Al) undergoes two distinct phase transitions induced by CO_2 between 273 and 318 K: $lp_{H_4} \rightarrow np_{H_4}$ below 1 bar and $np_{H_4} \rightarrow lp_{H_4}$ at higher pressures, as confirmed by our experimental data (Fig. 4A and B). In contrast, F_4-MIL-53(Al) displays Langmuir type isotherms below 1 bar in the same temperature range (Fig. 4C), consistent with a "classical" micropore filling. A clear step in the sorption profile is only observed at higher CO_2 pressures (Fig. 4D), with the step moving to lower pressure as the temperature decreases (from 8 bar at 313 K to 1 bar at 248 K). Plotting all CO_2 isotherms as a function of p/p_0, it can be observed that the step for each curve occurs between 0.07 and 0.1 p/p_0 and none of the explored temperatures reach this p/p_0 interval up to 1 bar (Fig. S14B). However, at 195 K the saturation pressure (p_0) of solid CO_2 is around 1 bar (1.9 bar considering CO_2 inside microporous channels as a supercooled liquid). Therefore, a larger range of relative pressure is explored, and the step is observed below 1 bar (Fig. S13). This step occurs at very low p/p_0 (~0.03), indicating a stronger interaction between CO_2 and the MOF at this temperature. Isotherms reported as a function of CO_2 relative pressure and the corresponding derivatives are shown in Fig. S14A. A linear trend between the temperature and the relative pressure at which the gate opening occurs is evident (Fig. S14C), allowing the estimation of the breathing pressure at a given temperature.

The CO_2-adsorption behaviour of F_4-MIL-53(Al) at room temperature differs from that reported by Van der Voort *et al.* for both F_1- and *para*F_2-MIL-53(Al),[25,26] which exhibited Langmuir-type CO_2 adsorption isotherms at 303 K in the 0–40 bar pressure range. The shape of the isotherms suggests that both partially fluorinated MOFs remain in their activated phases upon CO_2 adsorption. This is in contrast with the behaviour of F_4-MIL-53(Al), which presents an S-shaped isotherm under the same operating conditions, indicating a flexible response of the perfluorinated framework. However, since the breathing behaviour of MIL-53 has been shown to be highly sensitive to the synthetic procedure,[34] partially fluorinated MIL-53(Al) MOFs obtained by a hydrothermal rather than solvothermal (using DMF) synthetic procedure should be considered for a reliable comparison of the CO_2 induced flexibility in frameworks with different fluorination degrees.

Further investigation of the behaviour of F_4-MIL-53(Al) upon CO_2 adsorption was performed using several techniques, including microcalorimetry, PXRD, and IR and SS-NMR spectroscopies.
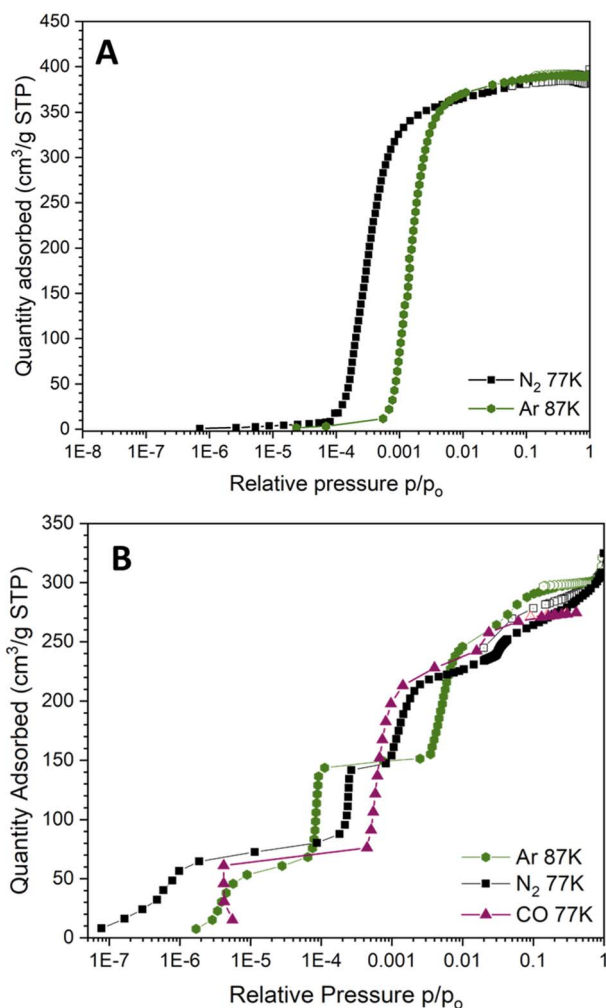

Fig. 3 Adsorption (full symbols) and desorption (empty symbols) isotherms in semi-logarithmic scale measured using Ar at 87 K (dark green hexagons), N_2 at 77 K (black squares) and CO at 77 K (purple triangles). (A) H_4-MIL-53(Al); (B) F_4-MIL-53(Al).

This journal is © The Royal Society of Chemistry 2025

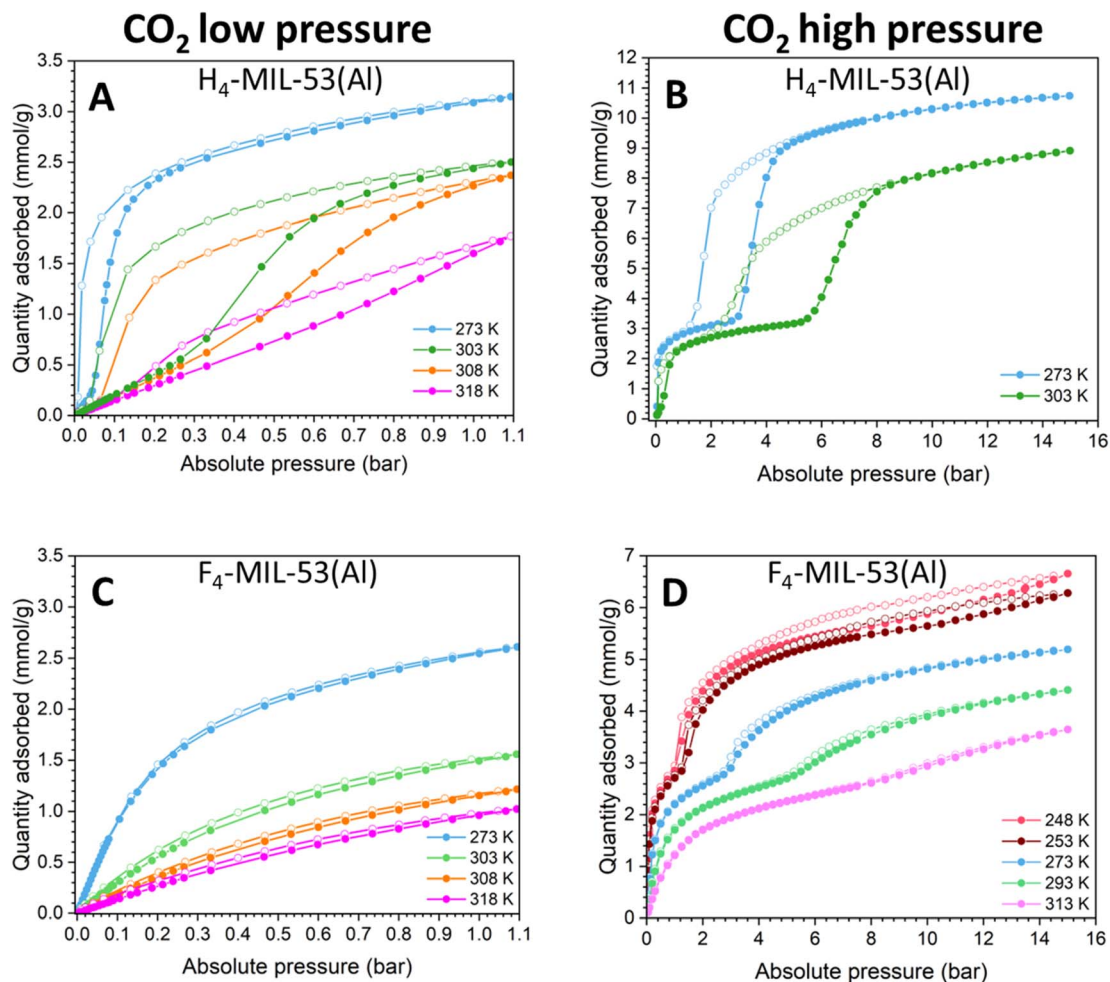*J. Mater. Chem. A*, 2025, **13**, 32446–32459 | **32451**

Fig. 4 CO_2 adsorption (full circles) and desorption (empty circles) isotherms performed at different temperatures. (A) H_4-MIL-53(Al) 0–1 bar; (B) H_4-MIL-53(Al) 0–16 bar; (C) F_4-MIL-53(Al) 0–1 bar; (D) F_4-MIL-53(Al) 0–16 bar.

For flexible structures, the adsorption enthalpy profile is characterised by endothermic phenomena due to structural transitions that counteract the exothermic adsorption process, resulting in a reduced neat total heat of adsorption.[46] The CO_2 adsorption enthalpy for F_4-MIL-53(Al) was directly measured at 273 K by adsorption microcalorimetry (Fig. 5A and B). At low CO_2 coverage, F_4-MIL-53(Al) displays values of heat of adsorption (Q_{st}) in the range of physisorption (30.6 kJ mol^{-1}). Q_{st} decreases as the pores (of the np_{F_4} phase) are loaded with CO_2 molecules (14.6 kJ mol^{-1} at 2.8 mmol g^{-1}). Notably, Q_{st} falls below the liquefaction heat of CO_2 (17 kJ mol^{-1}), suggesting that a modest contribution of an endothermic process is occurring and lowering the observed Q_{st}. At loadings higher than 3 mmol g^{-1} (p > 3 bar), Q_{st} suddenly rises to 20.5 kJ mol^{-1}. Indeed, at this pressure an $np_{F_4} \rightarrow c\_lp'_{F_4}$ (where c stands for "carbon dioxide") transition occurs, as evidenced by the step observed in the CO_2 isotherm at 273 K (Fig. 4D) and the PXRD pattern at high CO_2 pressure (Fig. 5D). Unfortunately, since calorimetric measurements report the total heat at a given CO_2 pressure resulting from both exothermic and endothermic events, they do not provide direct information about the strength of the interaction between the adsorbate and adsorbent immediately after the $np_{F_4} \rightarrow c\_lp'_{F_4}$ transition. The structural response of the F_4-MIL-53(Al) framework to CO_2 loading was investigated by collecting *in situ* PXRD patterns at 273 K in vacuum and at different CO_2 pressures between 0.05 and 2.2 bar (Fig. 5C). The unit cell of activated F_4-MIL-53(Al) is refined by Le Bail method in the orthorhombic crystal system (space group *Imam*, Fig. S15 and Table S1) with lattice parameters $a = 18.105(5)$ Å, $b = 10.621(2)$ Å and $c = 6.604(2)$ Å ($V = 1269.7(5)$ Å^3), which closely resemble those of the as synthesised material (np_{F_4}).[27] The increase of CO_2 loading up to 2 bar induces a small variation of the unit cell parameters, as clearly observed by the change of the 110 reflection at $2\theta = 9.60°$ (Fig. 5C). This reflection, corresponding to a d_{110} spacing of 9.20 Å, is associated to the 2D rhombohedral grid perpendicular to the channel axis (see Fig. S1C) and decreases to 8.97 Å at 0.5 bar (CO_2 uptake = 1.8 mmol g^{-1}), due to the newly formed CO_2 interactions with the framework. Contrarily, at higher loadings (p = 2.2 bar, CO_2 uptake = 2.6 mmol g^{-1}), an increase to 9.06 Å is detected, unveiling a homogeneous expansion of the unit cell of the framework (Fig. S16).
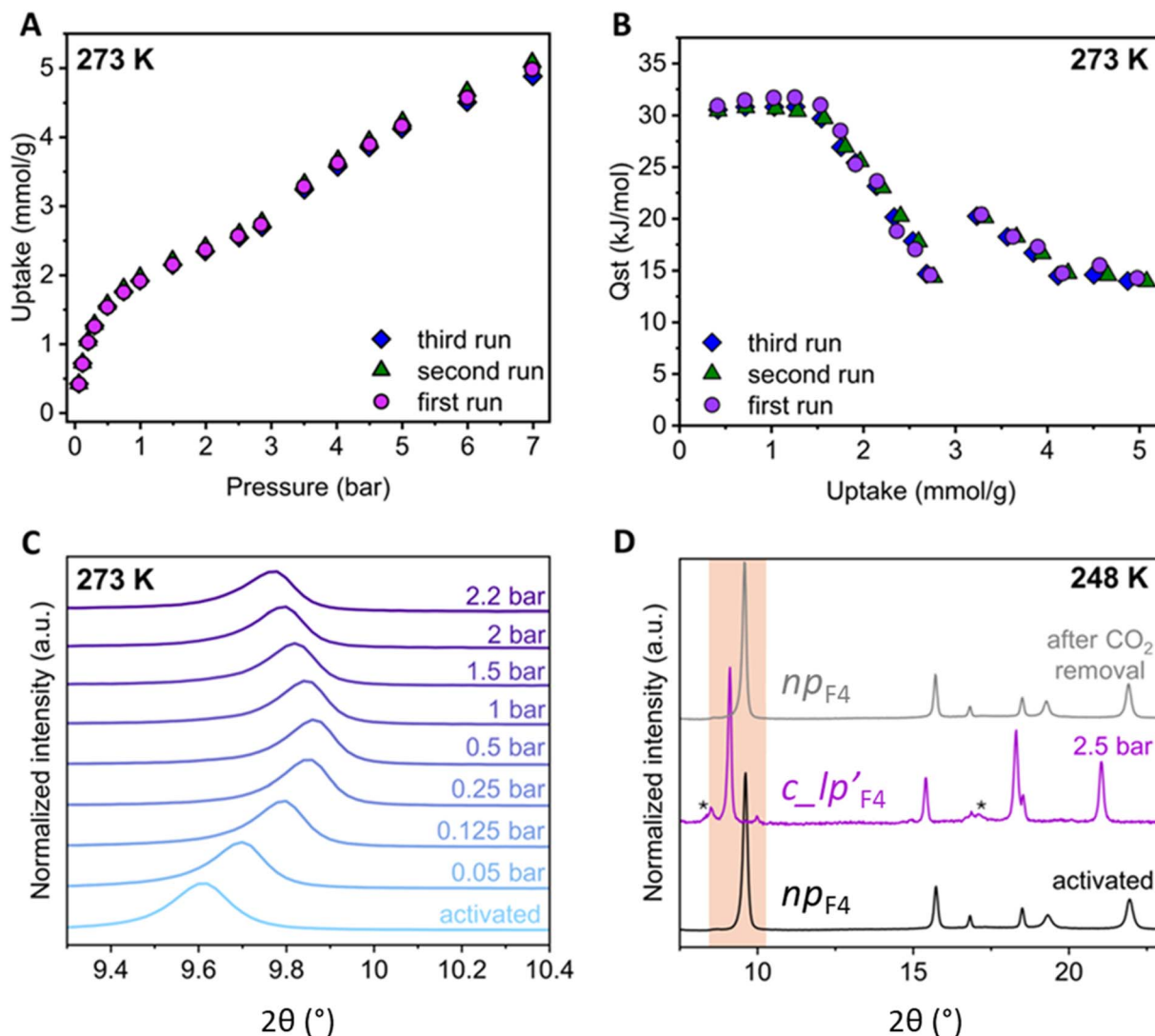
32452 | *J. Mater. Chem. A*, 2025, **13**, 32446–32459

This journal is © The Royal Society of Chemistry 2025

Fig. 5 CO_2 adsorption microcalorimetry and *in situ* PXRD patterns of F_4-MIL-53(Al) under controlled CO_2 pressure. (A) Volumetric adsorption isotherms of CO_2 collected up to 7 bar and 273 K coupled with microcalorimetry. The measurements were repeated three times on the same sample to reduce the experimental errors and prove reproducibility. (B) Isosteric heat of adsorption measured directly using adsorption microcalorimetry. (C) *In situ* PXRD patterns at low 2θ angles collected at 273 K at distinct CO_2 pressures. The main reflection corresponds to the 110 reflection and is diagnostic of the shrinkage and breathing behaviour of F_4-MIL-53(Al) upon CO_2 loading. (D) *In situ* PXRD patterns collected at 248 K on the activated sample, at 2.5 bar CO_2 loading, and after CO_2 removal. The asterisks indicate the peaks associated with a minor amount of c_lp phase.

Furthermore, to investigate the behaviour of F_4-MIL-53(Al) at higher CO_2 loadings, PXRD patterns were measured at 248 K and up to 2.5 bar (Fig. 5D). Remarkably, the diffraction pattern collected at 2.5 bar of CO_2 clearly shows a decrease in the symmetry of the unit cell, proving the occurrence of a phase transition induced by CO_2 from np_{F_4} to $c\_lp'_{F_4}$. The unit cell parameters are refined in the monoclinic crystal system, space group $I2/a$ ($a = 17.644(3)$ Å, $b = 11.521(2)$ Å, $c = 6.6026(8)$ Å and angle $\beta = 90.892(5)°$), showing a unit cell volume expansion to $1342.0(3)$ Å³ to accommodate the guest molecules and reaching a CO_2 loading value up to $\sim$4.7 mmol g^{-1}, as detected by the adsorption isotherm at 248 K (Fig. 4D). The phase transition is fully reversible, as demonstrated by the pattern collected on the sample after CO_2 removal under vacuum (Fig. 5D, S17–S19 and

Table S1). To complete the series, the *in situ* PXRD experiment was also performed at 293 K, but even the highest dose of CO_2 (2.5 bar) was insufficient to trigger any expansion of the unit cell (2.5 bar is indeed before the inflection point of the isotherm). The PXRD series at 293 K shows a slight contraction of the cell parameters associated with the generation of CO_2-framework interaction, similar to the results obtained at 273 K (Fig. S20).

Finally, the PXRD patterns of the F_4-MIL-53(Al) phases obtained by exposing the material to CO_2, H_2O and temperature in different conditions are directly compared in Fig. S21. A qualitative comparison of the $w\_lp'_{F_4}$ and $c\_lp'_{F_4}$ patterns reveals some differences between the two phases. In particular, the most intense reflection, appearing at lower angles in the case of $w\_lp'_{F_4}$, indicates a slightly more expanded cell. Regarding the lp
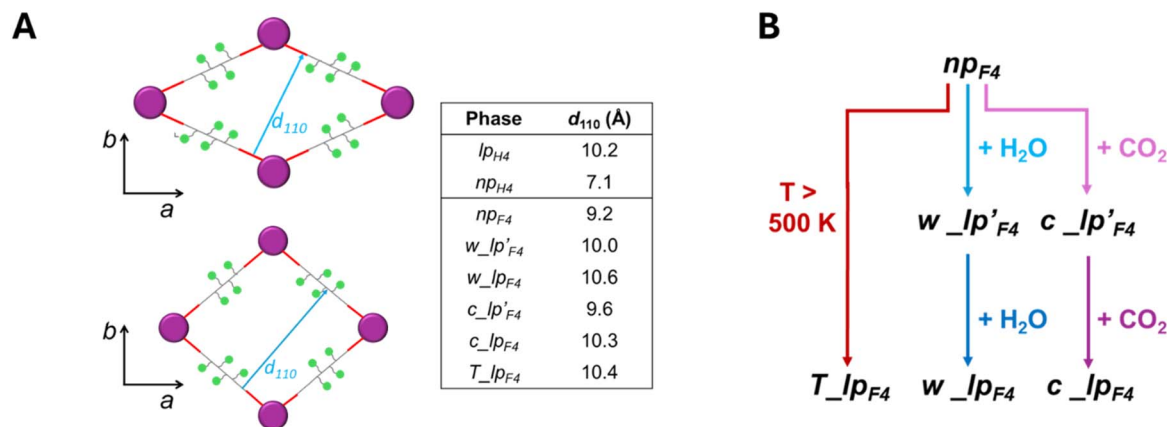
This journal is © The Royal Society of Chemistry 2025

J. Mater. Chem. A, 2025, **13**, 32446–32459 | **32453**

Fig. 6 (A) Schematic representation of the pore shape evolution of F_4-MIL-53(Al) from the np_{F_4} phase (rhombus shape, top) to the lp_{F_4} phases (square shape, bottom) induced by the elongation of the 110 distance (see table in panel A); (B) flow chart representing the different crystalline phases of F_4-MIL-53(Al) triggered by various stimuli (temperature, H_2O and CO_2 adsorption).

phases, even if it is not possible to directly compare the w_lp_{F_4} and the c_lp_{F_4} patterns, the presence of a c_lp_{F_4} phase is suggested by the weak signal appearing at low 2θ angles in the pattern acquired under 2.5 bar of CO_2 at 248 K (Fig. 5D); its complete detection was not achievable because of the instrumental limitations. Moreover, the more expanded monoclinic phase (w_lp_{F_4}) forming when the material is super hydrated (water soaking) can be compared to the temperature-induced expanded monoclinic phase (T_lp_{F_4}, where T stands for temperature), detectable upon heating the material above 500 K, as reported in our previous work.[27]

In situ IR spectroscopy was also employed to characterise F_4-MIL-53(Al) under incremental doses of CO_2 at RT and at the nominal temperature of 195 K (Fig. S22). The IR profile of F_4-MIL-53(Al) exhibits two signals at 1283 cm^{-1} and 1263 cm^{-1}, plus a shoulder around 1250 cm^{-1} with in-scale intensities. These bands may correspond to the deformation and in-plane bending modes of the fluorinated ring.[47] Hoffman *et al.* reported similar vibrational modes for the phenyl ring of H_4-MIL-53(Al) around 1000 cm^{-1}.[9,48] As shown in Fig. S22B, no shift is detected when CO_2 is adsorbed at RT. Contrarily, at 195 K, these bands clearly change (Fig. S22B'). A spectral fitting of these signals on the activated sample and at the maximum CO_2 coverage (Fig. S22C, D and Table S5) indicates that the higher frequency band only decreases in intensity, while those at 1264 cm^{-1} and 1253 cm^{-1} shift to higher wavenumbers upon CO_2 adsorption. To confirm the sensitivity of these bands to framework mobility, the same IR setup was employed to dose N_2 and CO at 77 K, and H_2O at RT. Fig. S23 shows a shift of the most intense band at the maximum coverage of H_2O, CO, or N_2. Notably, the shift with H_2O is smaller, likely due to the slow transition kinetics, indicating that the complete w_lp'_{F_4} phase is not reached. Another possibility is related to a temperature increase generated by the IR beam, locally decreasing the real RH value.

^{1}H, ^{19}F, ^{13}C, and ^{27}Al SS-NMR experiments were also performed on F_4-MIL-53(Al) and H_4-MIL-53(Al) samples loaded with 1 bar of $^{13}CO_2$ at 298 K. In agreement with the adsorption isotherms, only slight changes are detected in the spectra of CO_2-loaded F_4-MIL-53(Al) compared to the activated MOF (Fig. 2 and Tables S2–S4), indicating that no phase changes are observed upon CO_2 loading at 298 K. On the contrary, the adsorption of CO_2 considerably affects the ^{1}H, ^{13}C, and ^{27}Al SS-NMR spectra of H_4-MIL-53(Al) (Fig. S9 and Tables S2–S4), in agreement with data reported by Paula,[40] due to the lp_{H_4} to np_{H_4} phase transition. Indeed, for CO_2-loaded H_4-MIL-53(Al), shifts of both the aromatic and μ_2-OH proton signals and of the carboxyl carbon signals are observed compared to the activated MOF, analogous to those found when the phase transition is induced by hydration (lp_{H_4} to np_{H_4}). As far as the ^{27}Al spectrum is concerned, a slight variation in the isotropic chemical shift and C_q is observed, while η_Q shows a value similar to that observed for the hydrated sample (Table S3). Indeed, the alteration of δ and C_q values is most likely associated to changes in the charge distribution along the Al–OH axis, with μ_2-OH groups involved in the interactions with CO_2.[21,49] Conversely, the value of η_Q seems to be more influenced by the type of coordination of Al by carboxylate groups.[37,38]

The different structures of CO_2-loaded F_4-MIL-53(Al) and H_4-MIL-53(Al) also result in a different dynamics of CO_2. As shown by the static ^{13}C DE spectrum in Fig. S24, CO_2 (1 bar at 298 K) in F_4-MIL-53(Al) undergoes isotropic dynamics. Contrarily, for CO_2 in H_4-MIL-53(Al), ^{13}C MAS and static spectra typical of anisotropic dynamics are reported in the literature at room temperature, both in the np phase at low CO_2 pressure (below 6 bar) and in the lp phase at higher pressure.[50–52] These findings indicate that, at 298 K and 1 bar, no strong specific interactions of CO_2 with the framework of F_4-MIL-53(Al) occur, at variance with H_4-MIL-53(Al) in which stronger interactions of CO_2 with μ_2-OH groups constrain CO_2 molecules into specific orientations and restrict their dynamics. The greater mobility of the adsorbate in the np_{F_4} phase of F_4-MIL-53(Al) may also be due to its 30% larger volume compared to the CO_2-induced np_{H_4} phase of H_4-MIL-53(Al).

32454 | *J. Mater. Chem. A*, 2025, **13**, 32446–32459

This journal is © The Royal Society of Chemistry 2025

Overview of the multi-step breathing behaviour of F4-MIL-53(Al)

The multi-technique characterisation approach presented above provides key insights into the role of per-fluorination in modulating the breathing behaviour of MIL-53(Al). Beyond the previously reported temperature-induced breathing of F4-MIL-53(Al),[27] which profoundly diverges from the temperature-response of the hydrogenated analogue, we uncovered additional pronounced differences in adsorption-induced dynamic porosity. As summarised in Fig. 6, both CO_2 and H_2O trigger an expansion of the initial np_{F_4} phase, associated to the elongation of the d_{110} distance, which leads to a squaring of the pore shape (Fig. 6A). Moreover, as illustrated in the flow chart in Fig. 6B, the adsorption-induced breathing of F4-MIL-53(Al) follows a more intricate, multi-step mechanism. In order to facilitate the comprehension of the discrepancies between the breathing mechanisms of H4-MIL-53(Al) and F4-MIL-53(Al), the schematic illustration of the flexible behavior of the hydrogenated MOF is reported in Fig. S25.

Our study reveals the fundamental role of fluorine atoms in modifying the adsorption properties of the MIL-53(Al) framework and, most important, in affecting its breathing behaviour. Even if the mechanistic role of fluorine atoms is not clear, the different flexibility of the fluorinated framework could be associated with the modifications introduced by fluorine atoms on the organic linkers. Indeed, Férey *et al.* demonstrated that the aromatic rings of H4-MIL-53(Cr) undergo π flips about their C_2 symmetry axes with a normal Arrhenius process, thus triggering the transition. However, the rate and the activation energy of this motion are strongly dependent on the local geometry and electronic structure around the metal centre.[6,24,53,54] Fluorine substitution may affect both aspects, thus altering the overall flexible behaviour of fluorinated MIL-53.

Conclusions

This study provides the first comprehensive characterisation of the unique, multi-step adsorption-induced breathing behaviour of F4-MIL-53(Al), a new per-fluorinated Al-based MIL-53 analogue recently synthesised by our group. Through a systematic multi-technique *in situ* investigation and by directly comparing F4-MIL-53(Al) with its hydrogenated counterpart H4-MIL-53(Al), we unveiled the profound impact of fluorination on framework flexibility, adsorption properties, and phase transitions, offering new insights into the structure–property relationships governing dynamic porosity in MOFs.

Specifically, we revealed that F4-MIL-53(Al) undergoes complex phase transitions upon exposure to different adsorbates under various temperature and pressure conditions. More interacting species, such as H_2O and CO_2, trigger a cell expansion through a two-stage process, with the progressive conversion of the narrow pore np_{F_4} to intermediate lp'_{F_4} and, eventually, to large pore lp_{F_4} phases, as humidity or CO_2 pressure increase. This behaviour markedly diverges from the one of the hydrogenated H4-MIL-53(Al) analogue, for which the lp_{H_4} phase

collapses to np_{H_4} upon adsorption of H_2O or CO_2 (with a back-transformation to lp_{H_4} only at elevated CO_2 pressures).

Beyond H_2O and CO_2, a multi-step breathing has also been observed for F4-MIL-53(Al) upon adsorption of intermediate or weaker interacting probes (CO, N_2 and Ar), as highlighted by the unique multi-step adsorption isotherms measured at cryogenic temperatures.

Overall, this study highlights the critical role of ligand functionalisation (per-fluorination herein) in modulating the textural, adsorption and framework dynamic properties of MOFs, with an immediate impact on their macroscopic behaviour (*e.g.*, water affinity) and possible applications. The study also underscores the importance of a comprehensive *in situ* experimental approach to capture the rich, and often unexpected, adsorption-driven structural evolution of flexible MOFs, paving the way for the rational design of a new generation of stimuli-responsive porous materials with properties finely tuned for targeted applications.

Experimental

Materials

All chemicals are commercially available and used as received from the specified vendors without further purifications. Aluminium nitrate nonahydrate ($Al(NO_3)_3 \cdot 9H_2O$) was purchased from Honeywell Fluka™, tetrafluoroterephthalic acid (H_2-F4bdc) from SiKÉMIA, terephthalic acid (H_2-bdc) and $^{13}CO_2$ (^{13}C labeled CO_2; 99 at% ^{13}C) from Sigma Aldrich, and acetone from Merck.

Synthesis

For the synthesis of H4-MIL-53(Al), 0.57 g (3.4 mmol) of terephthalic acid (H_2-bdc) was dissolved in 9.8 mL of deionised water. In a second step, 2.55 g (6.8 mmol) of aluminium nitrate nonahydrate ($Al(NO_3)_3 \cdot 9H_2O$) was added. The mixture was put in a Teflon hydrothermal reactor and kept at 493 K for 72 h. The precipitated white solid was then washed twice with deionised water for 15 minutes. To remove the traces of trapped linker, the powder was heated in a muffle furnace at 603 K for 24 h. Yield: 50%.

F4-MIL-53(Al) was synthesised *via* a facile "solvent-free" method by mixing 3.75 g (10.0 mmol) of $Al(NO_3)_3 \cdot 9H_2O$ and 2.38 g (10.0 mmol) of tetrafluoroterephthalic acid (H_2-F4bdc) in a polytetrafluoroethylene (PTFE) hydrothermal reactor, which was kept at 393 K for 24 h. No solvent was added to the reactor, other than the hydration water of the aluminium precursor. The obtained mixture was washed twice with water for 15 minutes and finally with acetone. The recovered product was dried overnight in a static oven at 353 K. Yield: 82%.

Field emission scanning electron microscopy (FESEM)

FESEM images of F4-MIL-53(Al) and H4-MIL-53(Al) were acquired using a TESCAN S9000G FE-SEM 3010 microscope (30 kV), equipped with a Schottky type FEG source. Prior to analysis the samples were metalized with a chromium layer.

This journal is © The Royal Society of Chemistry 2025

J. Mater. Chem. A, 2025, **13**, 32446–32459 | **32455**

Powder X-ray diffraction (PXRD)

Powder X-ray diffractograms were collected on a PANalytical X'Pert diffractometer using Cu K$_\alpha$ radiation emitted by a cathode operated at 45 kV and 40 mA. To check the purity of H$_4$-MIL-53(Al) and the lack of traces of linker inside the pores, two patterns were collected in reflection geometry (2θ range = 5–30°), one before and one after the treatment in the muffle furnace at 603 K for 24 h.

To check the phase of F$_4$-MIL-53(Al) before and after evacuation, two diffractograms were acquired in Debye Scherrer geometry (2θ range = 5–30°), one directly on as-synthesized F$_4$-MIL-53(Al), the other after the capillary was kept at 423 K for 2 h under dynamic vacuum to remove physisorbed water. To check the different crystalline phases of the MOF exposed to about 75% RH, the capillaries were placed into an airtight chamber for several days together with a saturated solution of NaCl.

Variable temperature powder X-ray diffraction patterns of F$_4$-MIL-53(Al) were collected with a Rigaku powder diffractometer, equipped with a low-temperature chamber (Anton Paar TTK 600) operating with a liquid nitrogen cooling system, using Cu-Kα radiation, 40 kV, 30 mA over a range for 2θ of 7.0–40.0° with a step size of 0.02° and a scan speed of 1.0° min^{-1}. The chamber was equipped with vacuum and pressure transducers, connected to a gas (CO$_2$) line and a two-stage rotary pump to control the atmosphere inside the chamber. The as-synthesized sample was degassed *in situ* under high vacuum ($p < 1 \times 10^{-2}$ mmHg) at 423 K for 1 h. Then, the sample was cooled to the target temperature under vacuum and equilibrated for at least 30 min. The gas dosing was performed manually under isothermal conditions. The sample was equilibrated for 30 min and the PXRD diffraction patterns were collected. The dosing applied at the temperatures of 293 K, 273 K, and 248 K were reported in detail (Fig. S14, S17 and S18). The determination of the unit cell parameters, the identification of the space group, and the refinement of the unit cell parameters according to the Le Bail method were carried out with the EXPO2014 software.[55]

In situ Fourier Transform Infrared (FT-IR) spectroscopy

FT-IR measurements were collected within the 5000–500 cm^{-1} spectral range using a Bruker Vertex 70 spectrophotometer equipped with a MCT (mercury cadmium tellurium) cryogenic detector. The resolution of the reported IR spectra is 2.0 cm^{-1} and an average of 32 scans was used to enhance the signal to noise ratio. Before the analysis, the sample, in form of self-supported pellet mechanically protected by a gold envelope, was inserted in a home-made quartz cell with KBr windows. For experiments carried out at cryogenic temperatures, a special IR cell that can be filled with liquid nitrogen to lower the temperature of the system at about 100 K was employed.

To evaluate the optimal activation conditions, multiple spectra were acquired during *in situ* degassing at room temperature (RT) by using a conventional high-vacuum glass line, equipped with mechanical and turbo molecular pumps (residual pressure $p < 10^{-4}$ mbar). For F$_4$-MIL-53(Al), an additional *ex situ* treatment at 423 K for 2 h was necessary to completely remove water traces.

To investigate the interactions between the MOFs and different probes (*i.e.* CO$_2$, CO, N$_2$), the system was cooled down and multiple doses of gas (from 10^{-3} mbar to 10^2 mbar) were conveyed to the cell.

Low pressure gas sorption analysis

N$_2$ isotherms were collected at 77 K using a Micromeritics 3FLEX sorption analyser. The cooling bath was prepared using liquid nitrogen. For measurements on H$_4$-MIL-53(Al), 20 mg of sample was activated by heating overnight at 525 K (3 K min^{-1}) under dynamic vacuum, whereas in the case of F$_4$-MIL-53(Al), about 25 mg of powder was activated under dynamic vacuum at 423 K for 2 h (3 K min^{-1}). BET specific surface area (SSA) was evaluated following the Rouquerol consistency criteria[56] in the range 2×10^{-3} to 2×10^{-2} p/p_o and 6×10^{-3} to 4×10^{-2} p/p_o for H$_4$-MIL-53(Al) and F$_4$-MIL-53(Al), respectively.

For both materials, an Ar isotherm was collected at 87 K using a Micromeritics 3FLEX. The dewar was filled up with liquid argon. About 30 mg of sample was weighed and activated following the same procedures described above. The BET SSA was evaluated following the Rouquerol consistency criteria in the following ranges: 3×10^{-3} to 2×10^{-2} p/p_o for H$_4$-MIL-53(Al); 7×10^{-3} to 8×10^{-2} p/p_o for F$_4$-MIL-53(Al).

CO adsorption/desorption isotherms were acquired at 77 K on F$_4$-MIL-53(Al) using a Micromeritics ASAP2020 sorption analyser. The cooling bath was prepared using liquid nitrogen.

For both H$_4$-MIL-53(Al) and F$_4$-MIL-53(Al), CO$_2$ isotherms were collected at different temperatures in the 273–318 K range using a Micromeritics ASAP2020 sorption analyser. To keep isothermal conditions for each analysis, the sample was inserted in a home-made patented glass coating cell[57] in which a coolant or heating fluid, connected to a thermostatic bath (JULABO F25), can recirculate. About 60 mg of sample was weighed and activated following the already described procedures. A CO$_2$ isotherm was also collected at 195 K using a dry ice and isopropanol cooling bath.

High-pressure gas sorption analysis

High-pressure CO$_2$ and N$_2$ adsorption isotherms were measured on a Hiden IGA-001 gravimetric gas sorption analyser. The F$_4$-MIL-53(Al) sample was activated before the adsorption experiment at 423 K for 2 h under dynamic vacuum. The temperature of the analysis was controlled using a Julabo 600 F circulator.

Adsorption microcalorimetry

Gas adsorption isotherms up to 6 bar were collected on a volumetric adsorption analyser (Micromeritics ASAP 2050) in a high-pressure sample holder, while heat exchange was measured simultaneously with a Setaram μDSC7 Evo instrument at constant temperature ($T = 273$ K). The set-up allowed simultaneous determination of CO$_2$ adsorption isotherms and heat exchanged during the adsorption process at each adsorption step. Sorption-coupled microcalorimetry measurements were performed three times at 273 K, and the three different runs were averaged to reduce experimental errors. Data acquisition and processing were performed as detailed in the literature.[58,59]

32456 | *J. Mater. Chem. A*, 2025, **13**, 32446–32459

This journal is © The Royal Society of Chemistry 2025

Water adsorption/desorption isotherms

Water adsorption/desorption isotherms were collected at 303 K using a dynamic vapour sorption (DVS) analyser within a 0–90 relative humidity (RH%) range and a vapor flow of 20 sccm (standard cubic centimetres). About 40 mg of F_4-MIL-53(Al) and H_4-MIL-53(Al) were activated before the analysis under dynamic vacuum for 2 h at 423 K and 473 K, respectively.

Solid state NMR spectroscopy

SS-NMR experiments were carried out on a Bruker Avance Neo 500 spectrometer working at Larmor frequencies of 500.13, 470.59, 130.32, and 125.77 MHz for ^1H, ^{19}F, ^{27}Al, and ^{13}C nuclei, respectively, equipped with a double-resonance H-F/X 4 mm CP/MAS probe head.

^1H and ^{19}F spectra were recorded by Direct Excitation (DE) under magic angle spinning (MAS) conditions, accumulating 16 scans with a recycle delay between consecutive transients of 5–10 s and 3–15 s for ^1H and ^{19}F, respectively, depending on the sample. 90° pulse durations of 3.0 and 3.2 μs were employed for ^1H and ^{19}F, respectively. ^{19}F–^{13}C cross-polarization (CP) experiments were performed under MAS conditions and high power ^{19}F decoupling using a contact time of 2 ms and a recycle delay of 2–4 s and accumulating 200–400 scans depending on the sample. ^1H–^{13}C CP-MAS spectra were recorded under high power ^1H decoupling using a contact time of 2 ms and recycle delay of 2–6 s; 64–400 scans were accumulated depending on the sample. ^{13}C DE-MAS spectra were acquired with or without high power ^{19}F decoupling, using a recycle delay of 20 s and accumulating 128–24000 scans, depending on the sample. ^{27}Al DE-MAS spectra were acquired using an excitation pulse with a duration of 0.2 μs and accumulating 800–1600 scans with a recycle delay of 1 s.

If not otherwise stated, spectra were recorded at 298 K at a MAS frequency of 15 kHz using air as spinning gas. The chemical shift of all nuclei was referenced to the ^{13}C signal of adamantane at 38.48 ppm and calculated from the same value for all the other nuclei using the unified scale recommended by IUPAC.[60]

Line shapes of ^{27}Al DE-MAS spectra were analysed using the SOLA routine for line shape analysis implemented in Bruker TopSpin software.

Activated and CO_2 loaded samples were prepared using a home-made cell provided with a mechanical lever operated from outside enabling the capping of the rotor without disturbing the cell atmosphere. F_4-MIL-53(Al) and H_4-MIL-53 samples were activated by heating overnight under vacuum (0.1 mbar) at the temperature of 423 K the powder packed into the NMR rotor (4 mm external diameter) and closing the rotor under N_2 atmosphere. For the CO_2-loaded samples, the activated MOF was loaded with either CO_2 or $^{13}CO_2$ at 1 bar pressure and the rotor was capped under the gas atmosphere after equilibrium was reached.

Hydrated F_4-MIL-53(Al) was prepared by exposing the activated powder packed into the NMR rotor to either 75% RH or 100% RH atmosphere for different periods. At selected times, the sample was weighed to determine the amount of adsorbed water and the rotor was closed to perform measurements. Hydrated H_4-MIL-53(Al) was prepared by exposing the activated powder to the ambient atmosphere for 12 h.

A "wet" F_4-MIL-53(Al) sample was also prepared by adding 200 μL of H_2O to 100 mg of the MOF powder and packing the obtained hard paste into the NMR rotor.

Author contributions

V. G.: investigation, formal analysis, methodology, data curation, writing – original draft, writing – review & editing, visualisation; M. S. N.: investigation; J. P.: investigation, formal analysis, visualisation, writing – original draft, writing – review & editing; D. M. V.: investigation, formal analysis; F. N.: investigation, formal analysis, visualisation, writing – original draft; A. R.: investigation; S. B.: supervision; S. G.: supervision, resources; M. T.: formal analysis, writing – review & editing; M. S.: supervision, data curation; A. C.: supervision, writing – review & editing, resources; L. C.: investigation, formal analysis, visualisation, writing – original draft, supervision, resources, writing – review & editing, funding acquisition; F. C.: conceptualisation, writing – review & editing, supervision, resources, funding acquisition; V. C.: conceptualisation, writing – review & editing, supervision, funding acquisition, froject administration.

Conflicts of interest

There are no conflicts of interest to declare.

Data availability

All data for this article are available at Zenodo at **https://zenodo.org/communities/dam4co2/** with the identifier **https://doi.org/10.5281/zenodo.15429774**. Some data supporting this article have been included as part of the SI (all isotherms in AIF format).

Supplementary information is available: structural models of hydrated H_4-MIL-53(Al) and F_4-MIL53(Al); PXRD patterns of H_4-MIL-53(Al) and F_4-MIL-53(Al) after synthesis; FE-SEM images of H_4-MIL-53(Al) and F_4-MIL-53(Al); PXRD patterns of F_4-MIL-53(Al) as-synthesised and evacuated under dynamic vacuum for 2h at 423 K; *in situ* IR spectra of H_4-MIL-53(Al) and F_4-MIL53(Al) during evacuation at room temperature; Le Bail refinement of the PXRD diffraction pattern of water-soaked F_4-MIL-53(Al); Le Bail refinement outputs of the PXRD patterns of F_4-MIL-53(Al) under different temperature/adsorption conditions; ^1H and ^{19}F DE-MAS NMR spectra recorded at different times during the hydration of F_4-MIL-53(Al) at 75% and at 100% RH; isotropic chemical shift and number of hydrogens per formula for the different signals in the ^1H NMR spectra of activated, hydrated, and CO_2-loaded H_4-MIL-52(Al) and F_4-MIL-53(Al); ^{27}Al DE-MAS NMR spectra recorded at different times during the hydration of F_4-MIL-53(Al) at 75% RH; values of isotropic chemical shift, quadrupolar coupling constant and asymmetry parameter from ^{27}Al NMR spectra of H_4-MIL-52(Al) and F_4-MIL-53(Al); ^1H DE-MAS, ^1H-^{13}C CP-MAS, and ^{27}Al DE-MAS NMR spectra of

This journal is © The Royal Society of Chemistry 2025

J. Mater. Chem. A, 2025, **13**, 32446–32459 | **32457**

activated, hydrated and CO_2-loaded H_4-MIL-53(Al); N_2 (77 K) and Ar (87 K) adsorption/desorption isotherms of H_4-MIL-52(Al) and F_4-MIL-53(Al); BET fits of N_2 (77 K) and Ar (87 K) adsorption/ desorption isotherms of H_4-MIL-52(Al) and F_4-MIL-53(Al); CO_2 adsorption/desorption isotherms of F_4-MIL-53(Al) at 195 K; CO_2 adsorption isotherms of F_4-MIL-53(Al) measured at different temperatures and relation of gate-opening with temperature; Le Bail refinement of the PXRD diffraction pattern of F_4-MIL-53(Al) collected under dynamic vacuum at 273 K; CO_2 adsorption/ desorption isotherms of F_4-MIL-53(Al) collected at 273 K and *in situ* PXRD collected at significant CO_2 pressure values; Le Bail refinement of the PXRD diffraction pattern of F_4-MIL-53(Al) collected under dynamic vacuum and under 2.5 bar of CO_2 at 248 K; CO_2 adsorption/desorption isotherms of F_4-MIL-53(Al) collected at 248 K and *in situ* PXRD collected at significant CO_2 pressure values; CO_2 adsorption/desorption isotherms of F_4-MIL-53(Al) collected at 298 K and *in situ* PXRD collected at significant CO_2 pressure values; comparison of the PXRD patterns of the different phases of F_4-MIL-53(Al); CO_2 adsorption isotherms of F_4-MIL-53(Al) at room temperature and 195 K and *in situ* IR collected at significant CO_2 pressure values at both temperatures (including bands fit and related parameters); N_2 (77 K), CO (77 K) and H_2O (298 K) adsorption isotherms of F_4-MIL-53(Al) and *in situ* IR collected at significant adsorbent pressure values; static ^{13}C DE NMR spectrum of $^{13}CO_2$-loaded F_4-MIL-53(Al) at 298 K; schematic representation of the pore shape evolution of H_4-MIL-53(Al) under different stimuli. See DOI: **https://doi.org/10.1039/d5ta04373e**.

Acknowledgements

References

1 A. Schneemann, V. Bon, I. Schwedler, I. Senkovska, S. Kaskel and R. A. Fischer, *Chem. Soc. Rev.*, 2014, **43**, 6062–6096.

2 G. Férey and C. Serre, *Chem. Soc. Rev.*, 2009, **38**, 1380–1399.

3 D. Maspoch, D. Ruiz-Molina, K. Wurst, N. Domingo, M. Cavallini, F. Biscarini, J. Tejada, C. Rovira and J. Veciana, *Nat. Mater.*, 2003, **2**, 190–195.

4 C. Volkringer, T. Loiseau, N. Guillou, G. Férey, E. Elkaïm and A. Vimont, *J. Chem. Soc., Dalton Trans.*, 2009, 2241–2249.

5 S. Bourrelly, B. Moulin, A. Rivera, G. Maurin, S. Devautour-Vinot, C. Serre, T. Devic, P. Horcajada, A. Vimont, G. Clet, M. Daturi, J.-C. Lavalley, S. Loera-Serna, R. Denoyel,

P. L. Llewellyn and G. Férey, *J. Am. Chem. Soc.*, 2010, **132**, 9488–9498.

6 D. I. Kolokolov, H. Jobic, A. G. Stepanov, V. Guillerm, T. Devic, C. Serre and G. Férey, *Angew. Chem., Int. Ed.*, 2010, **49**, 4791–4794.

7 S. Tomar and V. K. Singh, *Mater. Today: Proc.*, 2021, **43**, 3291–3296.

8 Y. Liu, J.-H. Her, A. Dailly, A. J. Ramirez-Cuesta, D. A. Neumann and C. M. Brown, *J. Am. Chem. Soc.*, 2008, **130**, 11813–11818.

9 A. E. J. Hoffman, J. Wieme, S. M. J. Rogge, L. Vanduyfhuys and V. Van Speybroeck, *Z. Kristallogr. - Cryst. Mater.*, 2019, **234**, 529–545.

10 J. M. Salazar, G. Weber, J. M. Simon, I. Bezverkhyy and J. P. Bellat, *J. Chem. Phys.*, 2015, **142**, 124702.

11 T. M. McDonald, J. A. Mason, X. Kong, E. D. Bloch, D. Gygi, A. Dani, V. Crocellà, F. Giordanino, S. O. Odoh, W. S. Drisdell, B. Vlaisavljevich, A. L. Dzubak, R. Poloni, S. K. Schnell, N. Planas, K. Lee, T. Pascal, L. F. Wan, D. Prendergast, J. B. Neaton, B. Smit, J. B. Kortright, L. Gagliardi, S. Bordiga, J. A. Reimer and J. R. Long, *Nature*, 2015, **519**, 303–308.

12 Z. Zheng, A. H. Alawadhi, S. Chheda, S. E. Neumann, N. Rampal, S. Liu, H. L. Nguyen, Y. Lin, Z. Rong, J. I. Siepmann, L. Gagliardi, A. Anandkumar, C. Borgs, J. T. Chayes and O. M. Yaghi, *J. Am. Chem. Soc.*, 2023, **145**, 28284–28295.

13 C. Serre, F. Millange, C. Thouvenot, M. Noguès, G. Marsolier, D. Louër and G. Férey, *J. Am. Chem. Soc.*, 2002, **124**, 13519–13526.

14 T. Loiseau, C. Serre, C. Huguenard, G. Fink, F. Taulelle, M. Henry, T. Bataille and G. Férey, *Chem.—Eur. J.*, 2004, **10**, 1373–1382.

15 Y. Liu, Y. Li, F. Zuo, J. Liu, Y. Xu, L. Yang, H. Zhang, H. Wang, X. Zhang, C. Liu, Q. Li and H. Li, *Small*, 2022, **18**, 2203236.

16 M. Gaab, N. Trukhan, S. Maurer, R. Gummaraju and U. Müller, *Microporous Mesoporous Mater.*, 2012, **157**, 131–136.

17 A. López-Olvera, J. A. Zárate, E. Martínez-Ahumada, D. Fan, M. L. Díaz-Ramírez, P. A. Sáenz-Cavazos, V. Martis, D. R. Williams, E. Sánchez-González, G. Maurin and I. A. Ibarra, *ACS Appl. Mater. Interfaces*, 2021, **13**, 39363–39370.

18 A. Boutin, M.-A. Springuel-Huet, A. Nossov, A. Gédéon, T. Loiseau, C. Volkringer, G. Férey, F.-X. Coudert and A. H. Fuchs, *Angew. Chem., Int. Ed.*, 2009, **48**, 8314–8317.

19 A. Boutin, F.-X. Coudert, M.-A. Springuel-Huet, A. V Neimark, G. Férey and A. H. Fuchs, *J. Phys. Chem. C*, 2010, **114**, 22237–22244.

20 P. Mishra, H. P. Uppara, B. Mandal and S. Gumma, *Ind. Eng. Chem. Res.*, 2014, **53**, 19747–19753.

21 C. Serre, S. Bourrelly, A. Vimont, N. A. Ramsahye, G. Maurin, P. L. Llewellyn, M. Daturi, Y. Filinchuk, O. Leynaud, P. Barnes and G. Férey, *Adv. Mater.*, 2007, **19**, 2246–2251.

22 A. S. Munn, R. S. Pillai, S. Biswas, N. Stock, G. Maurin and R. I. Walton, *Dalton Trans.*, 2016, **45**, 4162–4168.

32458 | *J. Mater. Chem. A*, 2025, **13**, 32446–32459

This journal is © The Royal Society of Chemistry 2025

23 Z. Hulvey, E. Ayala and A. K. Cheetham, *Z. Anorg. Allg. Chem.*, 2009, **635**, 1753–1757.

24 S. Pakhira, M. Takayanagi and M. Nagaoka, *J. Phys. Chem. C*, 2015, **119**, 28789–28799.

25 S. Biswas, S. Couck, D. Denysenko, A. Bhunia, M. Grzywa, J. F. M. Denayer, D. Volkmer, C. Janiak and P. Van Der Voort, *Microporous Mesoporous Mater.*, 2013, **181**, 175–181.

26 S. Biswas, T. Rémy, S. Couck, D. Denysenko, G. Rampelberg, J. F. M. Denayer, D. Volkmer, C. Detavernier and P. Van Der Voort, *Phys. Chem. Chem. Phys.*, 2013, **15**, 3552–3561.

27 D. Morelli Venturi, V. Guiotto, R. D'Amato, L. Calucci, M. Signorile, M. Taddei, V. Crocellà and F. Costantino, *Mol. Syst. Des. Eng.*, 2023, **8**, 586–590.

28 K. Tan, N. Nijem, Y. Gao, S. Zuluaga, J. Li, T. Thonhauser and Y. J. Chabal, *CrystEngComm*, 2015, **17**, 247–260.

29 M. Shivanna, A. A. Bezrukov, V. Gascón-Pérez, K. Otake, S. Sanda, D. J. O'Hearn, Q.-Y. Yang, S. Kitagawa and M. J. Zaworotko, *ACS Appl. Mater. Interfaces*, 2022, **14**, 39560–39566.

30 C. Lieder, S. Opelt, M. Dyballa, H. Henning, E. Klemm and M. Hunger, *J. Phys. Chem. C*, 2010, **114**, 16596–16602.

31 G. Ortiz, G. Chaplais, J.-L. Paillaud, H. Nouali, J. Patarin, J. Raya and C. Marichal, *J. Phys. Chem. C*, 2014, **118**, 22021–22029.

32 B. Henry and A. Samokhvalov, *Spectrochim. Acta, Part A*, 2022, **267**, 120550.

33 J. Liu, B. Li, V. Martins, Y. Huang and Y. Song, *J. Phys. Chem. C*, 2024, **128**, 8007–8015.

34 W. P. Mounfield and K. S. Walton, *J. Colloid Interface Sci.*, 2015, **447**, 33–39.

35 H. Zhang, F. Xiao, H. Han and Y. Wu, *J. Membr. Sci.*, 2025, **713**, 123261.

36 Th. Emmler, S. Gieschler, H. H. Limbach and G. Buntkowsky, *J. Mol. Struct.*, 2004, **700**, 29–38.

37 A. E. Khudozhitkov, S. S. Arzumanov, A. V Toktarev, S. V Cherepanova, A. A. Gabrienko, D. I. Kolokolov and A. G. Stepanov, *Phys. Chem. Chem. Phys.*, 2021, **23**, 18925–18929.

38 B. Ibrahim, B. E. G. Lucier, J. Xu, P. He and Y. Huang, *Can. J. Chem.*, 2015, **93**, 960–969.

39 R. Giovine, C. Volkringer, J. Trébosc, J.-P. Amoureux, T. Loiseau, O. Lafon and F. Pourpoint, *Acta Crystallogr., Sect. C: Cryst. Struct. Commun.*, 2017, **73**, 176–183.

40 C. Paula, In situ solid-state NMR and XRD investigations of structural transformations in crystalline porous solids, PhD thesis, FAU University, 2021.

41 J. Tang, Y. Chu, S. Li, J. Xu, W. Xiong, Q. Wang and F. Deng, *Chem.–Eur. J.*, 2021, **27**, 14711–14720.

42 A. Datar, S. Yoon, L. C. Lin and Y. G. Chung, *Langmuir*, 2022, **38**, 11631–11640.

43 M. Thommes, K. Kaneko, A. V. Neimark, J. P. Olivier, F. Rodriguez-Reinoso, J. Rouquerol and K. S. W. Sing, *Pure Appl. Chem.*, 2015, **87**, 1051–1069.

44 M. Thommes and C. Schlumberger, *Annu. Rev. Chem. Biomol. Eng.*, 2021, **12**, 137–162.

45 K. Stracke and J. D. Evans, *J. Phys. Chem. C*, 2025, **129**, 3226–3233.

46 M. Cavallo, C. Atzori, M. Signorile, F. Costantino, D. M. Venturi, A. Koutsianos, K. A. Lomachenko, L. Calucci, F. Martini, A. Giovanelli, M. Geppi, V. Crocellà and M. Taddei, *J. Mater. Chem. A*, 2023, **11**, 5568–5583.

47 F. Li, Z. Zheng, S. Xia and L. Yu, *J. Mol. Struct.*, 2020, **1219**, 128480.

48 A. E. J. Hoffman, L. Vanduyfhuys, I. Nevjestić, J. Wieme, S. M. J. Rogge, H. Depauw, P. Van Der Voort, H. Vrielinck and V. Van Speybroeck, *J. Phys. Chem. C*, 2018, **122**, 2734–2746.

49 N. A. Ramsahye, G. Maurin, S. Bourrelly, P. L. Llewellyn, C. Serre, T. Loiseau, T. Devic and G. Férey, *J. Phys. Chem. C*, 2008, **112**, 514–520.

50 Y. Zhang, B. E. G. Lucier and Y. Huang, *Phys. Chem. Chem. Phys.*, 2016, **18**, 8327–8341.

51 S. Bin Baek and H. C. Lee, *Bull. Korean Chem. Soc.*, 2016, **37**, 588–591.

52 T. Kurihara, Y. Sori, K. Ikeda and M. Mizuno, *J. Phys. Chem. Lett.*, 2025, **16**(19), 4683–4688.

53 S. Pakhira, *RSC Adv.*, 2019, **9**, 38137–38147.

54 N. Sinha, I. Deshpande and S. Pakhira, *ChemistrySelect*, 2019, **4**, 8584–8592.

55 A. Altomare, C. Cuocci, C. Giacovazzo, A. Moliterni, R. Rizzi, N. Corriero and A. Falcicchio, *J. Appl. Crystallogr.*, 2013, **46**, 1231–1235.

56 J. Rouquerol, P. Llewellyn and F. Rouquerol, *Stud. Surf. Sci. Catal.*, 2007, **160**, 49–56.

57 V. Crocellà, C. Atzori, G. Latini, M. Signorile, A Kit for Volumetric Measurements of Gas Adsorption, WO Pat. 2021181211A1, 2021.

58 J. Perego, C. X. Bezuidenhout, A. Pedrini, S. Bracco, M. Negroni, A. Comotti and P. Sozzani, *J. Mater. Chem. A*, 2020, **8**, 11406–11413.

59 W. K. Feldmann, K.-A. White, C. X. Bezuidenhout, V. J. Smith, C. Esterhuysen and L. J. Barbour, *ChemSusChem*, 2020, **13**, 102–105.

60 R. K. Harris, E. D. Becker, S. M. Cabral De Menezes, R. Goodfellow and P. Granger, *Concepts Magn. Reson.*, 2002, **14**, 326–346.

This journal is © The Royal Society of Chemistry 2025

J. Mater. Chem. A, 2025, **13**, 32446–32459 | **32459**